RESEARCH ARTICLE

Development of a Lizard-Inspired Wall-Climbing Robot Using Pressure Sensitive Adhesion

SATYENDRA R. NISHAD[1], RAJU HALDER[2], (Member, IEEE),
GOURINATH BANDA[3], (Member, IEEE), AND ATUL THAKUR[1], (Member, IEEE)
[1]Department of Mechanical Engineering, Indian Institute of Technology Patna, Bihta, Bihar 801106, India
[2]Department of Computer Science and Engineering, Indian Institute of Technology Patna, Bihta, Bihar 801106, India
[3]Centre for Industrial Electronics, Department of Mechanical and Electrical Engineering, University of Southern Denmark, 6400 Sønderborg, Denmark

Corresponding author: Atul Thakur (athakur@iitp.ac.in)

ABSTRACT This paper presents the design, fabrication, and control of a quadruped wall-climbing robot. The robot's kinematics is inspired by lizards, which use trot-gait for the locomotion. The key features of this robot are its pressure-sensitive adhesive (PSA) enabled adhesion and peeling mechanism and the locomotion controller capable of straight and turning motion. We obtained an average vertical climbing speed of 1.35 cm/s without payload and 1.25 cm/s with a payload of 20 gm. Rapid prototyping techniques namely 3D-printing and 2D-LASER cutting are used to fabricate the entire structure of the robot, allowing easy replication of the entire robot in case a swarm of such robots is needed. This paper also reports climbing stability criteria for the developed robot expressed in terms of the pitching moment. We envisage that the developed robot can be deployed in surveillance, reconnaissance, cleaning, and repairing applications.

INDEX TERMS Bio-inspired robotics, climbing robots, lizard-inspired, 3D-printing.

I. INTRODUCTION

Robots having wall climbing capabilities with payloads such as cameras can be very useful in a wide range of applications like surveillance, reconnaissance, cleaning, repairing, and entertainment [1]. For example, consider a hostage situation where terrorists have captured a few innocent people, as depicted in Figure 1. This situation is very difficult to tackle for the security forces, as the information about the crisis scene, such as: the number of terrorists, kinds of weapons with them, and the number of hostages are not accurately known. While tackling this kind of situation, existing technologies such as drones fail miserably due to their inherent loud noise [2]. Wall-climbing, in particular, lizard-like robots can provide necessary stealth in security applications. Their small size, quiet and nimble operation, and house lizard-like appearance make them almost undetectable at the crisis scene, possibly saving many innocent lives. To this aim,

The associate editor coordinating the review of this manuscript and approving it for publication was Giulio Reina.
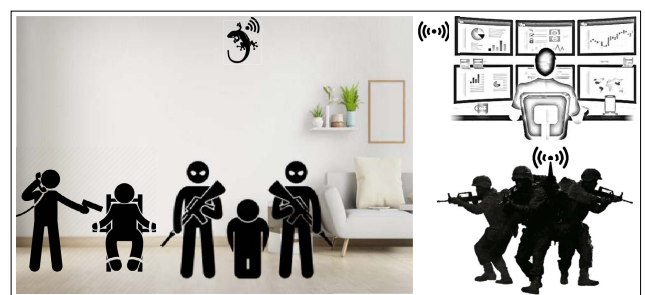
FIGURE 1. Lizard-inspired robot performing reconnaissance in hostage scenario.

in this paper, we present the design, fabrication, and control of a PSA-enabled lizard-like quadruped wall-climbing robot.

Crucial ethological functionality can be imparted to robots by having a robot design inspired by biological creatures [1], [3]–[6]. The complete robot design is inspired from the anatomy and nimble locomotion of a real lizard. 3D-printing [7] and 2D-LASER cutting [8] operations are used to fabricate the robot structure. The robot's limbs have a

simplified 2-DOF (degrees of freedom) design rather than the 3-DOF design naturally found in real lizards [9]. This simplification is done in order to reduce the complexity during fabrication and material selection for the robot. Micro servo motors of mass 9 gm and torque capacity 1.8kg-cm are used to actuate the leg joints. The motors on the spine provide yaw motion for the forward and steering motions, whereas the footpads assist in the adhesion and peeling of feet.

While designing climbing robots, the locomotion mechanism and the adhesion modality both play a crucial role. Researchers have attempted various adhesion modalities such as magnetic adhesion [10]–[21], electrostatic adhesion [22], [23], vacuum suction [24]–[29], micro spines [30]–[33], pressure-sensitive adhesion, and microfibrillar dry adhesion [34]–[39]. Each adhesion modality has its own advantages and disadvantages. For example, magnetic adhesion can work very well on ferromagnetic surfaces, but it cannot be used on other types of surfaces. Electrostatic adhesion generally needs a very high voltage and large pad size to generate the adhesion. Hence, the complete setup is usually bulky, and the untethered operation is difficult to achieve. Vacuum suction works well on smooth surfaces, but it fails on rough surfaces. Another issue is that since it needs ambient pressure in order to stick, it is not suitable for space applications as the ambient pressure is zero.

Chattopadhyay *et al.* [1] have done a comprehensive survey of various adhesion modalities for climbing-robots.

Researchers have also explored various locomotion mechanisms for climbing-robots [33]. Locomotion mechanisms such as legged [17], [34], [35], [38], [40], wheeled [10]–[14], [16], [24], [25], [41], [42], and tracked [15], [23], [26], [43] are most common. Again, each with its own advantages and disadvantages. Tracked and wheeled locomotions perform better on smooth surfaces, but they struggle on surfaces having obstacles and discontinuities, whereas legged locomotion works for a wide range of surfaces and it is better at negotiating the obstacles.

Tracked and wheeled locomotion for shipping and maritime robotics is explored in [12], [20], [21]. In legged locomotion, a quadruped robot design is widely used. Robots such as NINJA series [29], LEMUR-3 [44], REST [18], and ASTERISK [19] are examples of quadrupeds, whereas RiSE [31] is a bio-inspired hexapedal robot. Stickybot [38] and Geckobot [40], [45] are other quadrupedal robots that are inspired from a real lizard. Apart from the quadrupedal design, hexapedal design is also explored in [46]. This hexapedal design is inspired by a real spider that utilizes four front feet and two rear feet for its locomotion. There are three different versions of this robot, namely Abigaille-I, II, and III.

This paper reports a lizard-inspired quadrupedal design that uses PSA as the adhesion modality. This robot follows a trot-gait and has six servo-controlled motors, two for front and rear leg swinging and the remaining four for sticking and peeling the feet.

This paper is an extension of our earlier work [47] that reported preliminary results related to the design of a
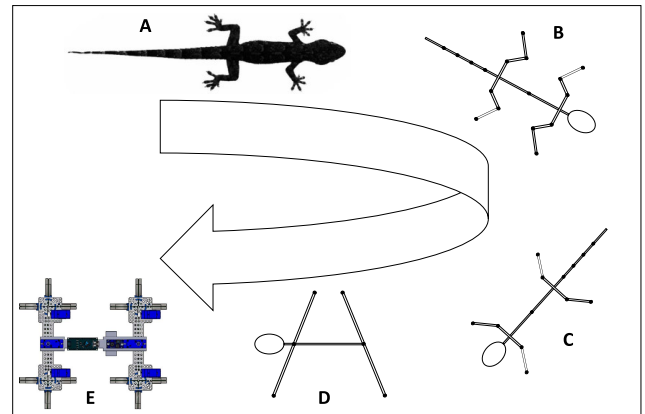
FIGURE 2. Design concept based on bio-inspiration [22]: (A) morphology of lizard having flexible body and tail, (B) robot design realization via flexibility of body and tail implemented using several revolute joints and incorporation of legs having 3-DOF, (C) robot design realization via flexibility of body and tail implemented using several revolute joints and incorporation of legs having 2-DOF, (D) further simplification of design by incorporating a pair of servo-actuated hip joints controlled via coupled oscillator, 1-DOF footpads, and rigid body devoid of tail, and (E) the realized robot.

lizard-inspired climbing robot. The main contributions of this paper include the following:

- A detailed climbing stability analysis based on pitching moment has been performed in this paper. The developed stability criteria helps in design improvement such that the robot can climb vertical surfaces in a stable manner.
- We report construction and simulation of the robot model in CoppeliaSim [48] environment.
- The paper includes results of Line of Sight (LoS) guidance to follow waypoints on a vertical wall in CoppeliaSim [48] environment.
- We report a new experiment in which the robot is carrying an on-board spy camera. The robot is able to climb vertically while recording video and streaming it online.

II. DESIGN OVERVIEW
A. DESIGN INSPIRATION FROM LIZARD MORPHOLOGY
Real lizards have a very flexible and compliant body with 3-DOF leg designs and a long tail, enabling them to have agile and nimble locomotion on vertical walls. While making a lizard-inspired robot, having all the above-said features is quite difficult. However, a simplified design can be a practical approach. In this paper, a simplified robot design with bionic locomotion based on the anatomy and nimble locomotion of a real lizard is developed.

As seen in Figure 2, a real lizard's body (Figure 2(A)) is simplified to have Figure 2(B) and Figure 2(C) in which flexibility of body and tail is obtained using multiple revolute joints. Figure 2(C) is further simplified to get Figure 2(D) in which, the body is made rigid, the legs have only 2-DOF, and the tail is omitted. Such simplifications have significantly reduced the overall complexity, power requirements, and weight as fewer actuators are utilized.
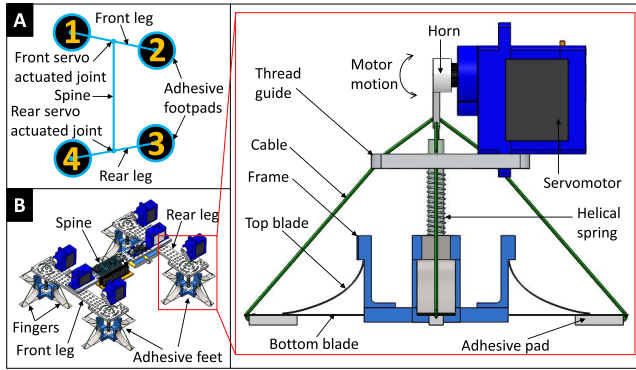
FIGURE 3. Robot design: (A) schematic diagram of the robot mechanism, and (B) CAD model of the robot with enlarged foot.

B. ROBOT DESIGN

The robot has three main structural components: spine, front leg, and rear leg (see Figure 3(A)). The front and rear legs are connected to the spine through a servo-actuated joint. These front and rear servo-actuated joints help in the leg swinging, thus generating the robot's front, rear, and steering motions. Each leg consists of two servo-actuated compliant adhesive feet at its ends.

The schematic diagram (see Figure 3(A)) is detailed in the CAD model [49] (see Figure 3(B)). As it can be seen in the CAD model, the spine houses all the electronics, power supplies, and the front and the rear servo motors.

Each leg has two compliant adhesion and peeling mechanisms, which mimic the toe-and-claw of a real lizard. The mechanism is inspired from the fact that a PSA adhesive peeling is very easy when pulled from a corner or an edge than peeling from its center. The overall design of the sticking and peeling mechanism is detailed in Figure 3. It consists of four compliant fingers, adhesive pads, foot frame, a helical spring, inextensible threads, and a servo motor. Each compliant finger has a top blade and a bottom blade. The top blade applies pressure on the adhesive pad, whereas the bottom blade acts as a substrate for attaching the adhesive pad. Each compliant finger is connected to the servo motor horn through a thread. While peeling, the servo motor pulls the compliant fingers from the edge with the help of threads. While sticking, the servo motor releases the threads, and the compliant finger applies pressure on the adhesive pads. The helical spring helps in landing the foot frame first before all four fingers can land; this helps in achieving a better adhesion.

The overall size of the robot can be encompassed in a bounding box of size 190 mm × 170 mm × 60 mm, its overall weight is 150 gm.

The kinematic analysis of the robot is shown below. At an instant, when one of the diagonal pair of feet is in contact with the ground, the robot structure behaves as a four bar mechanism as shown in Figure 4(A). From Figure 4(A), the vector distance between point A and D can be found as follows:

$$l_2 e^{i\theta_3} + L e^{i\theta_2} + l_1 e^{i\theta_1} = \overrightarrow{AD}, \tag{1}$$
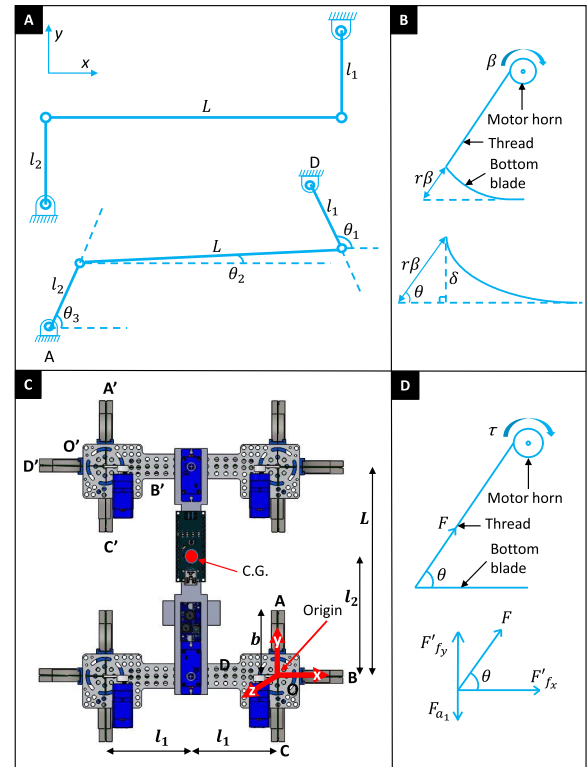
FIGURE 4. Kinematic and dynamic analysis: A) kinematic diagram of the robot [40], B) kinematic relationship between motor rotation and finger-tip height, C) Top view of the robot for pitching moment analysis, and D) dynamic relationship between motor torque and peeling force.

where, L represents the length of spine, l_1 represents the front leg width, l_2 represents the rear Leg width, θ_1 represents the angle made by l_1 from x axis, θ_2 represents the angle made by L from x axis, and θ_3 represents the angle made by l_2 from x axis.

Changing $\overrightarrow{AD}$ to its complex form, equation (1) can be rewritten as:

$$l_2 e^{i\theta_3} + L e^{i\theta_2} + l_1 e^{i\theta_1} = L + i\,(l_1 + l_2) \tag{2}$$

Equating real parts of equation (2), we get,

$$l_2 \cos\theta_3 + l_1 \cos\theta_1 = L - L\cos\theta_2 \tag{3}$$

Equating imaginary parts of equation (2), we get,

$$l_2 \sin\theta_3 + l_1 \sin\theta_1 = (l_1 + l_2) - L\sin\theta_2 \tag{4}$$

The rear motor rotation angle is $180 - \theta_3 + \theta_2$ and the front motor rotation angle is $\theta_1 - \theta_2$. Further, the step size can be calculated by using the following equation:

$$S = 2l_2 \cos\theta_3 \tag{5}$$

So, S can be determined by measuring the step size of the leg, and by substituting S in equation (5), θ_3 can be determined. θ_1 and θ_2 can be computed by solving equation (3) and (4).

The kinematic relationship between motor rotation and finger deflection is shown in Figure 4(B). When motor rotates

by an angle β, the thread connected between servo horn and finger-tip gets shortened by $r\beta$ length. The relationship between finger-tip height and thread length is given as follows:

$$\sin\theta = \frac{\delta}{r\beta} \Rightarrow \delta = (r\beta)\sin\theta, \qquad (6)$$

where, δ represents finger-tip height, r represents the motor shaft radius, β represents motor rotation angle, and θ represents the initial angle between thread and bottom blade of the finger. θ represents the initial angle between thread and bottom blade of the finger.

The dynamics analysis of the robot is shown below as per Figure 4(C). At first, the moment balance analysis of the robot is done in which, the conditions for pitching moment of the robot is derived as shown below.

The expression for moment of rear-foot ($ABCD$) and front-foot ($A'B'C'D'$) about Center of Gravity (CoG) is shown in equation (7) and equation (8) respectively:

$$\overrightarrow{M_{G_r}} = 4\left[-R_{r_z}l_2 + R_{r_y}l_3\right]\hat{i} - 4R_{r_z}l_1\hat{j} + 4R_{r_y}l_1\hat{k} \qquad (7)$$

$$\overrightarrow{M_{G_f}} = 4\left[R_{f_z}(L-l_2) + R_{f_y}l_3\right]\hat{i} + 4R_{f_z}l_1\hat{j} - 4R_{f_y}l_1\hat{k} \qquad (8)$$

where, M_{G_r} represents moment of rear-foot about CoG, M_{G_f} represents moment of front-foot about CoG, R_{r_y} represents the net force on each rear-footpad in y direction, R_{r_z} represents the net force on each rear-footpad in z direction, R_{f_y} represents the net force on each front-footpad in y direction, R_{f_z} represents the net force on each front-footpad in z direction, l_1 represents the distance of CoG from origin in x direction, l_2 represents the distance of CoG from origin in y direction, l_3 represents the distance of CoG from origin in z direction.

For stability, $\overrightarrow{M_G} \leq 0 \Rightarrow \overrightarrow{M_{G_r}} + \overrightarrow{M_{G_f}} \leq 0$, so, by comparing the coefficients of the given equation, we get the following relations:

$$\frac{R_{f_z}L + \left(R_{r_y} + R_{f_y}\right)l_3}{R_{r_z} + R_{f_z}} \leq l_2 \qquad (9)$$

$$R_{f_z} < R_{r_z} \qquad (10)$$

$$R_{r_y} < R_{f_y} \qquad (11)$$

Referring Figure 4(D), the relationship between motor torque and peeling force is shown as follows. Applying force balance about a single finger we get the following relationships:

$$F_{a_1} = \left(\frac{\tau}{r}\right)\sin\theta + F'_{f_y} \qquad (12)$$

$$F'_{f_x} = \left(-\frac{\tau}{r}\right)\cos\theta, \qquad (13)$$

where, τ represents servo motor torque, F represents the thread tension, r represents the motor shaft radius, F'_{f_y} represents normal reaction on a single footpad, F'_{f_x} represents net frictional force on a single footpad, F_{a_1} represents adhesion force acting on a single footpad, θ represents angle between thread and bottom blade of the finger.

The adhesion/peeling force models are described below as seen in Figure 5. In the case of a smooth, rigid plate contacting
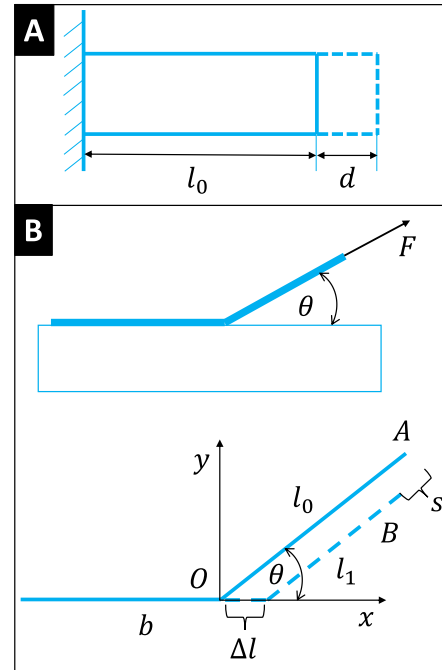

FIGURE 5. Adhesion/Peeling model: A) adhesion of an elastic block on a smooth surface, B) force diagram of a flexible adhesive tape acted on by an external force [50].

a smooth, elastic block (see Figure 5(A)), the block and the plate adhere to each other due to adhesive force, and a force must be applied to separate the block from the plate. If a force is applied at the free end of the block then a tensile stress σ will be induced that will lead to a stretching of the block by length d. The failure stress due to which the block separates from the rigid surface, is given by:

$$\sigma_{cr} = \sqrt{\frac{4\gamma E}{l_o}}, \qquad (14)$$

where, σ_{cr} represents critical stress, γ represents surface energy, E represents modulus of elasticity, and l_o represents thickness of the elastic block.

This "critical stress" increases with the modulus of elasticity E and the surface energy γ and decreases with the elastic block thickness l_o. In the case of adhesive tapes, condition for the equilibrium is discussed below. Consider a flexible adhesive tape having width L, which is partly adhered on a rigid body and partly in air, and it is being pulled with force F as seen in Figure 5(B).

The critical separation force is given by the following relation:

$$F_0 = \frac{\gamma^* L}{1 - \cos\theta}, \qquad (15)$$

where, F_0 represents critical separation force, γ^* represents the effective surface energy, L represents width of adhesive tape, and θ represents angle at which the tape is pulled.

The critical separation force (per unit length) when the adhesive tape is pulled at an angle $\theta = 90^o$, is equal to the surface energy. Whereas when $\theta = 180^o$, it is half as large.

C. FABRICATION OF THE ROBOT

Rapid prototyping techniques such as 3D-printing and 2D-LASER cutting are used for the fabrication of the complete robot structure. This enables easy replication of the entire robot prototype.

Robot feet are fabricated using the 3D-printing operation. First, all the small components of the feet frame are 3D printed using ABS (Acrylonitrile Butadiene Styrene) thermoplastic (see Figure 6(A-i)), and then they are glued together to form the foot frame as seen in Figure 6(A-ii). Low chromium stainless steel blades of thickness 0.09 mm are used to make the compliant fingers, which mimic the toe-claw fingers of a real lizard. First, the edges of the blades are made blunt using emery paper; after that, they are cut into the required shapes and sizes. Holes are punched in it to attach threads. These processed blades are finally inserted in the foot frame as a top and bottom blade and stuck with the superglue Figure 6(A-iii)). Finally, this setup is assembled on the front and the rear legs with helical springs and inextensible threads (see Figure 9).

Robot legs and spine are fabricated using the 2D-LASER cutting operation. A 3mm thick Polyoxymethylene (POM) thermoplastic sheet is used as the material. Perforations are made to reduce the overall weight of the robot (see Figure 6(B) and 6(C)).

Customized servo horns are made using the 2D-LASER cutting operation. Raster and Vector operations are performed on a 5mm thick Polyoxymethylene (POM) thermoplastic sheet to get the desired shape. Grooves are handcrafted on the top and the bottom sides of the horn using sharp cutting tools. When threads are tied using a special knot, these grooves help lock them to a specific length. (See Figure 6(D))

III. LOCOMOTION CONTROL

The robot uses a trot-based gait for its locomotion (see Figure 7(A)). This trot-based gait is realized using two movements: a) sticking and peeling movement of the feet and b) synchronized front and rear leg swinging. Each foot's sticking and peeling movement takes place with the help of a servo-actuated prismatic joint. In contrast, the synchronized front and rear leg swinging happen with the help of a servo-actuated revolute joint present between the spine and the leg. This synchronized front and rear leg swinging is produced using a pair of the phase-lagged coupled oscillator, whose equations are given below:

$$\theta_f = A\sin(\omega t) + \gamma \tag{16}$$

and

$$\theta_r = A\sin(\omega t + \pi) - \gamma, \tag{17}$$

where, θ_f represents angular-displacements of the front joint, θ_r represents angular-displacements of the rear joint, γ represents the offset from the neutral position, ω represents the joint actuation frequency, A represents the joint actuation amplitude, and t represents time.
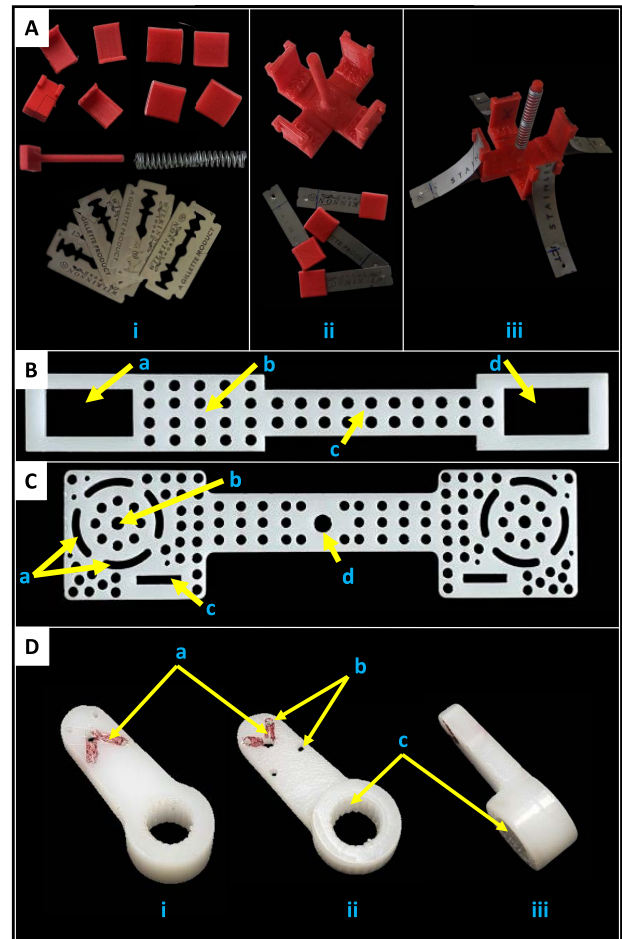
FIGURE 6. Fabrication: A) Foot: (i) basic components, (ii) 3D printed parts glued together, (iii) the final structure, B) Spine: a) slot for the rear servo motor, b) place for on-board power supply related electronics, c) place for the motor control shield, d) slot for the front servo motor, C) Legs: a) slots for threads, b) slot for foot frame cylinder, c) slot for foot servo motor, d) internal gear slot for front and back servo motor shaft, D) Servo horns: i) top view, i) bottom view, iii) side view, a) handcrafted grooves, b) holes through which threads pass, c) internal gear teeth.

A gait diagram is shown in Figure 7(B), in which one complete gait cycle is shown. On the x-axis, time is shown in milliseconds; similarly, on the y-axis, the footpad number is shown. Dark horizontal lines show the time for which a particular footpad is attached to the climbing surface (also known as support period). For the remaining time, the footpad remains detached from the climbing surface. Each footpad remains attached for 75% of the cycle time. So, the duty factor, which is a ratio of the support period and the cycle time [51] of each footpad is 75%.

For taking a left or right turn, the front and rear legs need to get offset w.r.t. the neutral position (see Figure 7(C)) in one particular direction. This offset is provided with the help of γ (see equations 16 and 17). However, choosing a γ value should ensure the following condition: $A + \gamma < min(M, \pi/2)$ which means the sum of the joint amplitude and the offset is smaller than the maximum displacement limit of the actuating servo motors and under no condition, the legs collide with the
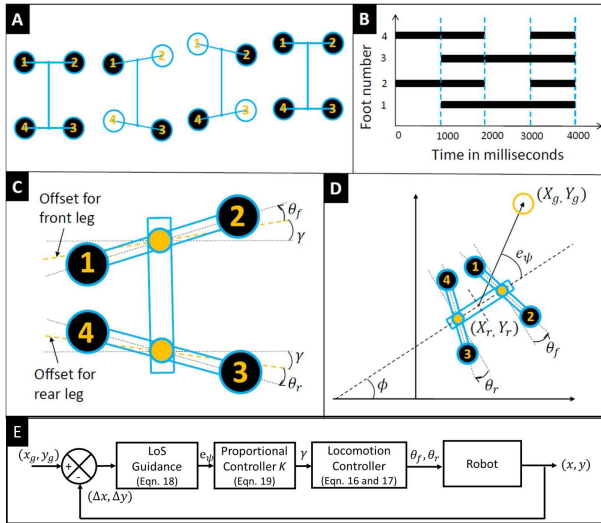
FIGURE 7. Control scheme for locomotion: (A) schematic of the trot-gait, (B) gait diagram, (C) actuation of front and rear legs, (D) guidance law based on LoS, and (E) an overview of controller feedback loop.

spine. Here, M represents the maximum displacement limit of the actuating servo motor.

LoS-based guidance technique is employed in this paper (see Figure 7(D)), in which first, the error e_ψ in terms of the angle between the robot's current position and the goal position is calculated. Then this error is used to find out the offset value γ as follows:

$$e_\psi = \text{atan}_2(y_g - y_r, x_g - x_r) - \phi \qquad (18)$$

$$\gamma = Ke_\psi, \qquad (19)$$

where, e_ψ represents the error, (x_r, y_r) represents point on the robot, (x_g, y_g) represents goal location, ϕ represents angle with horizontal axis, K represents proportional gain. The overall controller feedback loop has been shown in Figure 7(E).

Each servo-actuated joint (1.8 kg-cm torque capacity) is controlled with the help of an Arduino Nano Board [52], which has an Atmel Atmega328 microcontroller and the interfacing electronics in the form of a shield (see Figure 8). The shield is designed and fabricated inhouse on a two-sided Printer circuit board (PCB). The schematic and board view of the designed shield is shown in Figure 8(A) and 8(B). An on-board power supply is provided with a 2S 480mah Li-po battery which is stepped down to get a 5V regulated power supply with the help of a DC-DC buck converter. A 2.4GHz bluetooth module (HC05) is used for wireless communication between the robots and the command and control center. A spy camera of 5MP resolution is present on the robot for capturing the videos and live streaming it online. This camera setup is a combination of a Raspberry Pi Zero W board [53] and a 5MP OV5647 spy camera module. The spy camera module helps in capturing the video and the Raspberry Pi Zero W board helps in processing it and streaming it online.
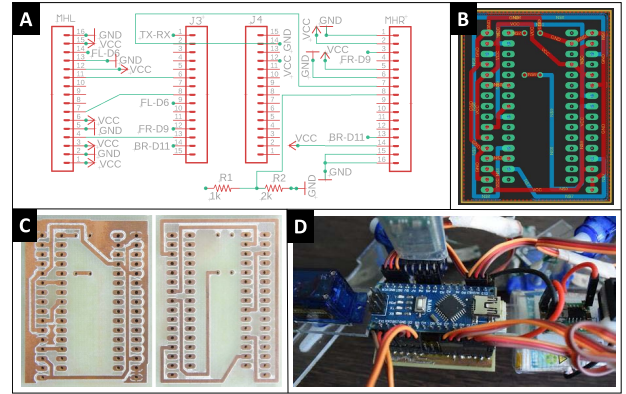
FIGURE 8. Motor control shield: A) schematic view of the circuit, B) board view of the circuit, C) top and bottom layers of the fabricated PCB, and D) fully assembled shield on the robot.
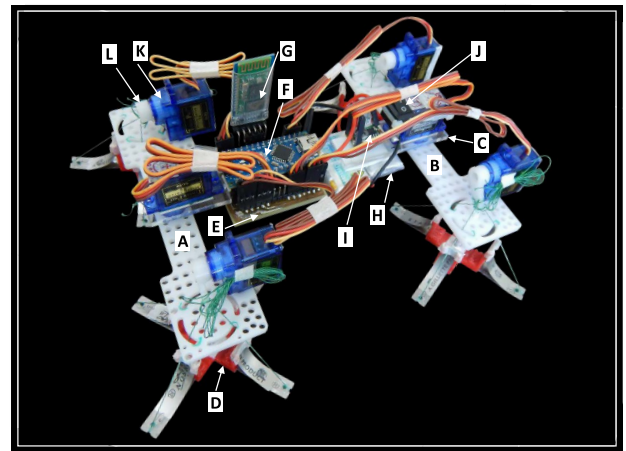
FIGURE 9. Fully assembled robot: A) front leg, B) rear leg, C) spine, D) sticky foot, E) motor control shield, F) Arduino-Nano Board, G) bluetooth module, H) lithium-polymer battery, I) dc-dc buck converter, J) power switch, K) micro servo motor, and L) custom made servo horn.

IV. EXPERIMENTAL RESULTS AND DISCUSSION

This section presents results of the following three experiments:

- vertical climbing with and without dead payload,
- vertical climbing with on-board spy camera, and
- modeling and LoS-based waypoint tracking in CoppeliaSim.

A fully fabricated and assembled robot is shown in Figure 9.

A. VERTICAL CLIMBING WITH AND WITHOUT DEAD PAYLOAD

An experimental climbing surface is created at PLANR[1] Laboratory for testing the climbing capabilities of the designed robot. The climbing surface is created with the help of a 60 cm long transparent acrylic sheet with distances marked on it. The climbing angle is set to 90°.

The offset value γ is set to 0, and the peak amplitude is kept as 20°. The duty factor of the trot-gait is set to 75%.

[1]Programming LANguages & Robotics (PLANR) Lab, IIT Patna
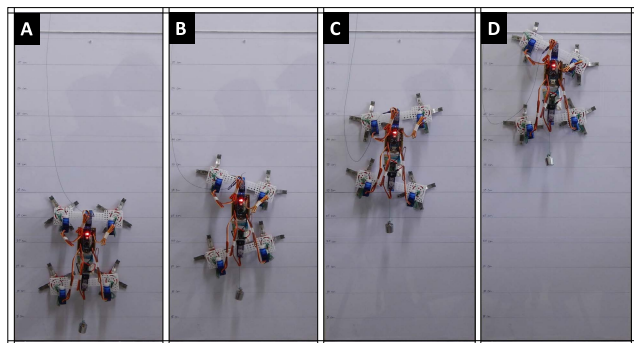
FIGURE 10. Snapshots of robot carrying a 20 gm payload while climbing a vertical surface at different times: (a) 0 sec, (b) 10 sec, (c) 20 sec, and (d) 28 sec. (See multimedia extensions 1 and 2).

The experiments are done in two phases. In the first phase, no payload is attached to the robot. Fresh adhesive pads are stuck to the fingers. The robot is placed on the climbing surface, and a command to move forward is issued. The robot climbs a distance of 35 cm (1.8 body length) in 25 sec with an average velocity of 1.4 cm/sec. Without replacing the adhesive pads, the experiment is repeated, and this time the robot could climb a distance of 26 cm (1.4 body length) in 20 sec with an average velocity of 1.3 cm/sec. In the second phase, a 20g payload is attached to the robot, and fresh adhesive pads are attached to the fingers. With this setting, the robot could climb a distance of 35 cm (1.8 body length) in 28 sec with a velocity of 1.25 cm/sec (see Figure 10). The videos of the above experiments can be viewed in multimedia extensions 1 and 2.

B. VERTICAL CLIMBING WITH ON-BOARD SPY CAMERA
Another experiment was performed with the same setup mentioned above where a Raspberry Pi Zero W board [53] along with a spy camera module is mounted on the robot (see Figure 11). Raspberry Pi Zero W board is placed on the spine, whereas the spy camera module is placed on the robot head. This setup is powered from the on-board power supply of the robot. The spy camera module used has a fixed focus with a native resolution of 5MP, maximum frame rate of 30fps, and a Field-of-view (FoV) of 64 x 48 degrees. It has a Camera Serial Interface (CSI) which connects directly to the Raspberry Pi Zero W board. The Raspberry Pi Zero W board has on-board wireless LAN (802.11 b/g/n) through which it can send the live video stream captured by the spy camera module to any client device connected to it. The overall weight of this setup was around 10g. The robot was able to climb the vertical surface with an average velocity of 1.09 cm/sec along with video recording and live streaming it online (see multimedia extension 3).

C. MODELING AND WAYPOINT TRACKING IN COPPELIASIM
A robot model is constructed and simulated in the CoppeliaSim environment (see Figure 12(A)). CoppeliaSim
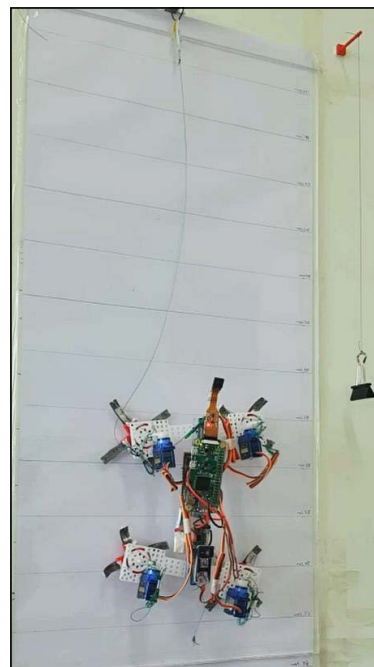

FIGURE 11. Vertical climbing with on-board spy camera. (See multimedia extension 3).

is a versatile, scalable, yet powerful general-purpose robot simulation framework [54].

At first, the SOLIDWORKS model of the robot is converted to the '.stl' file format. These '.stl' files are then imported as a mesh file in the CoppeliaSim environment. After that, CoppeliaSim specific changes are made so that the robot becomes respondable to the simulation environment. Revolute joints are added on the front and back side of the spine between front and the back legs. Prismatic joints are added between all four foot and each ends of the legs. To simulate the curling motion of the compliant fingers, the top and bottom blades are divided into multiple segments and these multiple segments are joined with each other with the help of revolute joints.

The adhesive pads are attached to the bottom blades with the help of dummy objects. Adhesion is achieved with the help of force element and proximity sensor. A combination of force element and proximity sensor is attached to each foot of the robot. The proximity sensor detects contact between the foot and the climbing surface. When the distance between the foot and the climbing surface is less than the threshold, the normal force is increased using the force element. By changing the normal force, the friction force acting between the foot and the surface can be altered, and it is assumed that this force acts as the adhesion force between the foot and the climbing surface. A Lua [55] script is written in order to move the robot from one point to the other point. A video of the simulated robot can be seen at multimedia extension 4.

In a different experiment, in the CoppeliaSim environment, a camera is attached to the robot. The robot is made to climb a vertical wall following a series of waypoints using the
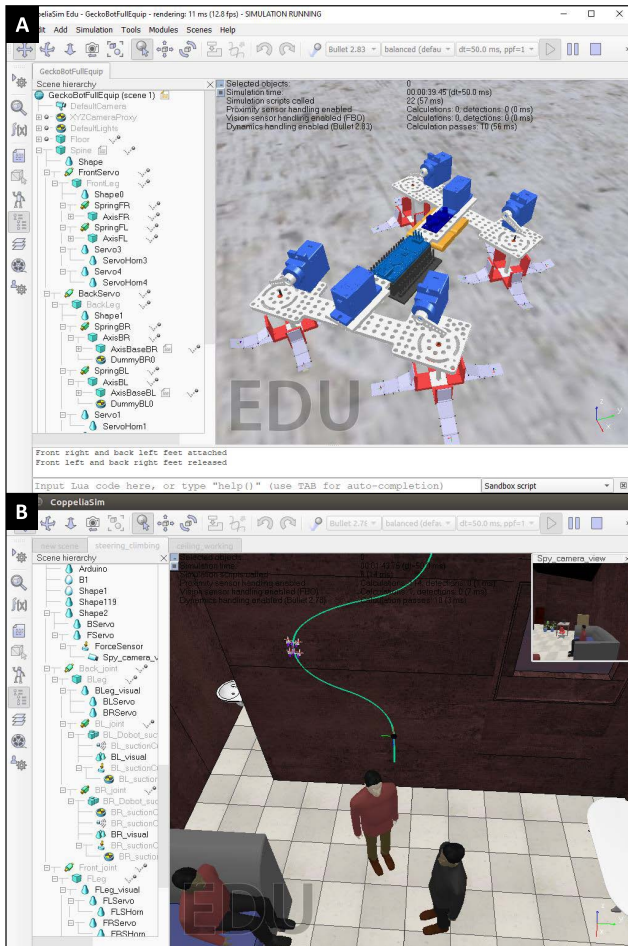
FIGURE 12. CoppeliaSim: A) robot model construction, B) LoS-based waypoint tracking with on-board spy camera. (See multimedia extensions 4 and 5).

LoS-based guidance technique (see Figure 12(B)). A vision sensor available in the CoppeliaSim is used as a camera, and it is mounted on the anterior portion of the robot in such a way that while climbing one wall in a room, it can easily see other walls. The camera used on the robot has a resolution of 512×512 pixels, and it has a FoV of $90° \times 90°$.

A realistic experimental setup of a closed room is created in the CoppeliaSim using the available 3D model objects like people, chairs, tables, windows, doors, and walls. Textures are added to make the room more realistic. Each 3D model object is set to be measurable, collidable, and detectable so that sensors can sense these objects. A path made up of waypoints is created on a wall using the path module available in the CoppeliaSim. These waypoints are used as an input to the controller for LoS-based guidance. The controller for LoS-based guidance is already described in this paper (see section III). An interface between the CoppeliaSim and the Robot Operating System (ROS) [56] is created in order to make the best use of both and exchange the required data between each other. CoppeliaSim captures videos through the robot camera and sends them to the ROS through a ROS topic to which ROS is subscribed. ROS can then use this video

stream for further processing. Similarly, ROS publishes robot joint angles calculated by the LoS-based guidance controller on a different ROS topic, and CoppeliaSim gets this data as it is subscribed to this ROS topic. These joint angles are then used to move the robot to follow the desired path. Multimedia extension 5 show the robot following waypoints while climbing.

V. CONCLUSION

We developed an untethered lizard-inspired quadruped wall climbing robot based on PSA adhesion. A new adhesion and peeling mechanism is designed and reported in this paper, which enables an easy attachment and detachment on the climbing surfaces. This paper also reports a climbing stability criteria based on pitching moment. A detailed simulation model of the robot with path following experiments has also been reported in this paper. The robot can climb on vertical walls with an average speed of 1.35 cm/s without payload and 1.25 cm/s with a payload of 20 gm. The robot can also carry a spy camera that can record videos and stream it online during vertical climbing. The entire robot is built using rapid prototyping techniques such as 3D-printing and 2D-LASER cutting, allowing quick replication, which will be useful for building a swarm of similar robots for surveillance applications.

We are currently in the process of further miniaturizing the robot and adding an active tail for better stability while climbing. To deal with dusty surfaces micro-fibrillar dry adhesives [36]–[38] may be incorporated for improved performance. Online video analytics can be performed for surveillance applications. We believe that the quiet operation of the developed lizard-inspired robot can inspire research on swarm of such robots which can be used in various applications such as surveillance and reconnaissance. Swarm of climbing robots can also find applications in cleaning, repairing, and space.

APPENDIX
MULTIMEDIA EXTENSIONS
Details of all the multimedia extension files are provided in Table 1.

TABLE 1. List of multimedia extension files.

Sr. No.	Video Files	Caption
1	1.wmv	Vertical climbing with dead payload
2	2.wmv	Vertical climbing without dead payload
3	3.wmv	Vertical climbing with on-board spy camera
4	4.wmv	Robot modeling and simulation in CoppeliaSim
5	5.wmv	LoS-based waypoint following in CoppeliaSim

REFERENCES

[1] P. Chattopadhyay and S. K. Ghoshal, "Adhesion technologies of bio-inspired climbing robots: A survey," *Int. J. Robot. Autom.*, vol. 33, no. 6, pp. 1–8, 2018, doi: 10.2316/JOURNAL.206.2018.6.206-5193.

[2] J.-P. Yaacoub, H. Noura, O. Salman, and A. Chehab, "Security analysis of drones systems: Attacks, limitations, and recommendations," *Internet Things*, vol. 11, Sep. 2020, Art. no. 100218, doi: 10.1016/J.IOT.2020.100218.

[3] A. A. Transeth, K. Y. Pettersen, and P. Liljebäck, "A survey on snake robot modeling and locomotion," *Robotica*, vol. 27, no. 7, pp. 999–1015, Dec. 2009, doi: 10.1017/S0263574709005414.

[4] B. Chu, K. Jung, C.-S. Han, and D. Hong, "A survey of climbing robots: Locomotion and adhesion," *Int. J. Precis. Eng. Manuf.*, vol. 11, no. 4, pp. 633–647, Aug. 2010, doi: 10.1007/s12541-010-0075-3.

[5] Q. Wu, C. Liu, J. Zhang, and Q. Chen, "Survey of locomotion control of legged robots inspired by biological concept," *Sci. China Ser. F, Inf. Sci.*, vol. 52, no. 10, pp. 1715–1729, Oct. 2009, doi: 10.1007/s11432-009-0169-7.

[6] A. Raj and A. Thakur, "Fish-inspired robots: Design, sensing, actuation, and autonomy—A review of research," *Bioinspiration Biomimetics*, vol. 11, no. 3, Apr. 2016, Art. no. 031001, doi: 10.1088/1748-3190/11/3/031001.

[7] B. Evans, *Practical 3D Printers: The Science and Art of 3D Printing*. New York, NY, USA: Apress, 2012.

[8] P. A. Hilton, "In the beginning: The history of laser cutting," in *International Congress on Applications of Lasers & Electro-Optics*, vol. 171727. Scottsdale, AZ, USA: Laser Institute of America, 2002.

[9] K. G. Karwa, S. Mondal, A. Kumar, and A. Thakur, "An open source low-cost alligator-inspired robotic research platform," in *Proc. 6th Int. Symp. Embedded Comput. Syst. Design (ISED)*, Dec. 2016, pp. 234–238.

[10] H. Eto and H. H. Asada, "Development of a wheeled wall-climbing robot with a shape-adaptive magnetic adhesion mechanism," in *Proc. IEEE Int. Conf. Robot. Autom. (ICRA)*, May 2020, pp. 9329–9335.

[11] M. Eich and T. Vogele, "Design and control of a lightweight magnetic climbing robot for vessel inspection," in *Proc. 19th Medit. Conf. Control Autom. (MED)*, Jun. 2011, pp. 1200–1205.

[12] R. E. Abdulkader, P. Veerajagadheswar, N. H. Lin, S. Kumaran, S. R. Vishaal, and R. E. Mohan, "Sparrow: A magnetic climbing robot for autonomous thickness measurement in ship hull maintenance," *J. Mar. Sci. Eng.*, vol. 8, no. 6, p. 469, Jun. 2020, doi: 10.3390/JMSE8060469.

[13] J. Shang, B. Bridge, T. Sattar, S. Mondal, and A. Brenner, "Development of a climbing robot for inspection of long weld lines," *Ind. Robot, Int. J.*, vol. 35, no. 3, pp. 217–223, May 2008, doi: 10.1108/01439910810868534.

[14] H. B. Santos, M. A. S. Teixeira, N. Dalmedico, A. S. de Oliveira, F. Neves-Jr., J. E. Ramos, and L. V. R. de Arruda, "Model predictive torque control for velocity tracking of a four-wheeled climbing robot," *Sensors*, vol. 20, no. 24, p. 7059, Dec. 2020, doi: 10.3390/S20247059.

[15] S. T. Nguyen and H. M. La, "A climbing robot for steel bridge inspection," *J. Intell. Robotic Syst.*, vol. 102, no. 4, pp. 1–21, Aug. 2021, doi: 10.1007/S10846-020-01266-1.

[16] M. A. S. Teixeira, H. B. Santos, N. Dalmedico, L. V. R. de Arruda, F. Neves, and A. S. de Oliveira, "Intelligent environment recognition and prediction for NDT inspection through autonomous climbing robot," *J. Intell. Robotic Syst.*, vol. 92, no. 2, pp. 323–342, Oct. 2018, doi: 10.1007/S10846-017-0764-6.

[17] T. Bandyopadhyay, R. Steindl, F. Talbot, N. Kottege, R. Dungavell, B. Wood, J. Barker, K. Hoehn, and A. Elfes, "Magneto: A versatile multi-limbed inspection robot," in *Proc. IEEE/RSJ Int. Conf. Intell. Robots Syst. (IROS)*, Oct. 2018, pp. 2253–2260.

[18] J. C. Grieco, M. Prieto, M. Armada, and P. Gonzalez de Santos, "A six-legged climbing robot for high payloads," in *Proc. IEEE Int. Conf. Control Appl.*, Sep. 2008, pp. 446–450.

[19] P. Kriengkomol, K. Kamiyama, M. Kojima, M. Horade, Y. Mae, and T. Arai, "New tripod walking method for legged inspection robot," in *Proc. IEEE Int. Conf. Mechatronics Autom.*, Aug. 2016, pp. 1078–1083.

[20] O. Kermorgant, "A magnetic climbing robot to perform autonomous welding in the shipbuilding industry," *Robot. Comput.-Integr. Manuf.*, vol. 53, pp. 178–186, Oct. 2018, doi: 10.1016/J.RCIM.2018.04.008.

[21] H. Huang, D. Li, Z. Xue, X. Chen, S. Liu, J. Leng, and Y. Wei, "Design and performance analysis of a tracked wall-climbing robot for ship inspection in shipbuilding," *Ocean Eng.*, vol. 131, pp. 224–230, Feb. 2017, doi: 10.1016/J.OCEANENG.2017.01.003.

[22] R. Chen, R. Liu, J. Chen, and J. Zhang, "A gecko inspired wall-climbing robot based on electrostatic adhesion mechanism," in *Proc. IEEE Int. Conf. Robot. Biomimetics (ROBIO)*, Dec. 2013, pp. 396–401.

[23] R. Liu, R. Chen, H. Shen, and R. Zhang, "Wall climbing robot using electrostatic adhesion force generated by flexible interdigital electrodes," *Int. J. Adv. Robotic Syst.*, vol. 10, no. 1, p. 36, Jan. 2013, doi: 10.5772/54634.

[24] A. Papadimitriou, G. Andrikopoulos, and G. Nikolakopoulos, "On the optimal adhesion control of a vortex climbing robot," *J. Intell. Robotic Syst.*, vol. 102, no. 3, p. 57, Jul. 2021, doi: 10.1007/S10846-021-01420-3.

[25] I. M. Koo, T. D. Trong, Y. H. Lee, H. Moon, J. Koo, S. K. Park, and H. R. Choi, "Development of wall climbing robot system by using impeller type adhesion mechanism," *J. Intell. Robotic Syst.*, vol. 72, no. 1, pp. 57–72, Oct. 2013, doi: 10.1007/S10846-013-9820-z.

[26] J. Zhu, D. Sun, and S.-K. Tso, "Development of a tracked climbing robot," *J. Intell. Robotic Syst.*, vol. 35, no. 4, pp. 427–443, 2002, doi: 10.1023/A:1022383216233.

[27] N. Ali, U. Zafar, S. Ahmad, J. Iqbal, and Z. H. Khan, "LizBOT design and prototyping of a wireless controlled wall climbing surveillance robot," in *Proc. Int. Conf. Commun. Technol. (ComTech)*, Apr. 2017, pp. 210–215.

[28] R. Lal Tummala, R. Mukherjee, N. Xi, D. Aslam, H. Dulimarta, J. Xiao, M. Minor, and G. Dang, "Climbing the walls [robots]," *IEEE Robot. Autom. Mag.*, vol. 9, no. 4, pp. 10–19, Dec. 2002, doi: 10.1109/MRA.2002.1160067.

[29] A. Nagakubo and S. Hirose, "Walking and running of the quadruped wall-climbing robot," in *Proc. IEEE Int. Conf. Robot. Autom.*, May 1994, pp. 1005–1012.

[30] S. Kim, A. T. Asbeck, M. R. Cutkosky, and W. R. Provancher, "SpinybotII: Climbing hard walls with compliant microspines," in *Proc. 12th Int. Conf. Adv. Robot. (ICAR)*, Jul. 2005, pp. 601–606.

[31] M. J. Spenko, G. C. Haynes, J. A. Saunders, M. R. Cutkosky, A. A. Rizzi, R. J. Full, and D. E. Koditschek, "Biologically inspired climbing with a hexapedal robot," *J. Field Robot.*, vol. 25, nos. 4–5, pp. 223–242, Apr. 2008, doi: 10.1002/ROB.20238.

[32] Q. Hu, E. Dong, and D. Sun, "Soft gripper design based on the integration of flat dry adhesive, soft actuator, and microspine," *IEEE Trans. Robot.*, vol. 37, no. 4, pp. 1065–1080, Aug. 2021, doi: 10.1109/TRO.2020.3043981.

[33] J. Xu, L. Xu, J. Liu, X. Li, and X. Wu, "Survey on bioinspired adhesive methods and design and implementation of a multi-mode biomimetic wall-climbing robot," in *Proc. IEEE/ASME Int. Conf. Adv. Intell. Mechatronics (AIM)*, Jul. 2018, pp. 688–693.

[34] M. Henrey, A. Ahmed, P. Boscariol, L. Shannon, and C. Menon, "Abigaille-III: A versatile, bioinspired hexapod for scaling smooth vertical surfaces," *J. Bionic Eng.*, vol. 11, p. 1–17, Jan. 2014, doi: 10.1016/S1672-6529(14)60015-9.

[35] A. Srisuchinnawong, B. Wang, D. Shao, P. Ngamkajornwiwat, Z. Dai, A. Ji, and P. Manoonpong, "Modular neural control for gait adaptation and obstacle avoidance of a tailless gecko robot," *J. Intell. Robotic Syst.*, vol. 101, no. 2, p. 27, Feb. 2021, doi: 10.1007/S10846-020-01285-y.

[36] B. Aksak, M. P. Murphy, and M. Sitti, "Gecko inspired micro-fibrillar adhesives for wall climbing robots on micro/nanoscale rough surfaces," in *Proc. IEEE Int. Conf. Robot. Autom.*, May 2008, pp. 3058–3063.

[37] H. K. Raut, A. Baji, H. H. Hariri, H. Parveen, G. S. Soh, H. Y. Low, and K. L. Wood, "Gecko-inspired dry adhesive based on micro–nanoscale hierarchical arrays for application in climbing devices," *ACS Appl. Mater. Interface*, vol. 10, no. 1, pp. 1288–1296, Jan. 2018, doi: 10.1021/ACSAMI.7b09526.

[38] S. Kim, M. Spenko, S. Trujillo, B. Heyneman, V. Mattoli, and M. R. Cutkosky, "Whole body adhesion: Hierarchical, directional and distributed control of adhesive forces for a climbing robot," in *Proc. IEEE Int. Conf. Robot. Autom.*, Apr. 2007, pp. 1268–1273.

[39] S. Kalouche, N. Wiltsie, H.-J. Su, and A. Parness, "Inchworm style gecko adhesive climbing robot," in *Proc. IEEE/RSJ Int. Conf. Intell. Robots Syst.*, Sep. 2014, pp. 2319–2324.

[40] O. Unver, A. Uneri, A. Aydemir, and M. Sitti, "Geckobot: A gecko inspired climbing robot using elastomer adhesives," in *Proc. IEEE Int. Conf. Robot. Autom. (ICRA)*, May 2006, pp. 2329–2335.

[41] M. P. Murphy, C. Kute, Y. Mengüç, and M. Sitti, "Waalbot II: Adhesion recovery and improved performance of a climbing robot using fibrillar adhesives," *Int. J. Robot. Res.*, vol. 30, no. 1, pp. 118–133, Jan. 2011, doi: 10.1177/0278364910382862.

[42] A. Parness and C. McKenzie, "DROP: The durable reconnaissance and observation platform," *Ind. Robot, Int. J.*, vol. 40, no. 3, pp. 218–223, Apr. 2013, doi: 10.1108/01439911311309906.

[43] O. Unver and M. Sitti, "Tankbot: A palm-size, tank-like climbing robot using soft elastomer adhesive treads," *Int. J. Robot. Res.*, vol. 29, no. 14, pp. 1761–1777, Dec. 2010, doi: 10.1177/0278364910380759.

[44] A. Parness, N. Abcouwer, C. Fuller, N. Wiltsie, J. Nash, and B. Kennedy, "LEMUR 3: A limbed climbing robot for extreme terrain mobility in space," in *Proc. IEEE Int. Conf. Robot. Autom. (ICRA)*, May 2017, pp. 5467–5473.

[45] O. Unver, M. Murphy, and M. Sitti, "Geckobot and Waalbot: Small-scale wall climbing robots," in *Infotech@Aerospace*. Reston, VA, USA: American Institute of Aeronautics and Astronautics, 2005.

[46] C. Menon, Y. Li, D. Sameoto, and C. Martens, "Abigaille-I: Towards the development of a spider-inspired climbing robot for space use," in *Proc. 2nd IEEE RAS EMBS Int. Conf. Biomed. Robot. Biomechatronics*, Oct. 2008, pp. 384–389.

[47] A. Thakur, R. Halder, G. Banda, R. Ray, A. Bhattacharya, and S. R. Nishad, "A lizard-inspired quadruped robot based on pressure sensitive adhesion mechanism for wall climbing," in *Proc. Adv. Robot. 5th Int. Conf. Robot. Soc.*, Jun. 2021, pp. 1–5.

[48] *CoppeliaSim Simulator*. Coppelia Robotics, Ltd. Accessed: Feb. 3, 2022. [Online]. Available: http://www.coppeliarobotics.com/

[49] *SOLIDWORKS*. Dassault Systmes. Accessed: Jun. 11, 2021. [Online]. Available: https://www.3ds.com/products-services/solidworks/

[50] V. L. Popov, *Contact Mechanics and Friction: Physical Principles and Applications*. Berlin, Germany: Springer, 2017.

[51] O. K. B. Siciliano, Ed., *Springer Handbook of Robotics*. Berlin, Germany: Springer, 2008.

[52] *Arduino Open Source Project*. Arduino. Accessed: Jun. 11, 2021. [Online]. Available: https://www.arduino.cc/

[53] *Raspberry Pi Zero W Board*. Raspberry Pi Foundation. Accessed: Feb. 15, 2022. [Online]. Available: https://www.raspberrypi.com/products/raspberry-pi-zero-w/

[54] E. Rohmer, S. P. N. Singh, and M. Freese, "V-REP: A versatile and scalable robot simulation framework," in *Proc. IEEE/RSJ Int. Conf. Intell. Robots Syst.*, Nov. 2013, pp. 1321–1326.

[55] *Lua Scripting Language*. Accessed: Feb. 4, 2022. [Online]. Available: http://www.lua.org/home.html

[56] *Robot Operating System (ROS)*. Accessed: Feb. 15, 2022. [Online]. Available: https://www.ros.org/

RAJU HALDER (Member, IEEE) received the Ph.D. degree from the Università Cá Foscari, Italy, in 2012. He is currently an Associate Professor with the Department of Computer Science and Engineering, IIT Patna. Before joining IIT Patna, he worked as a Postdoctoral Researcher at Macquarie University, Australia. He worked with the Robotics Team, HASLaboratory, University of Minho, Portugal, in 2016. Prior to his Ph.D., he worked as an Associate System Engineer at IBM India Pvt. Ltd., from 2007 to 2008. His research interests include formal methods, blockchain technology, robotics, and data privacy and security.

GOURINATH BANDA (Member, IEEE) received the Ph.D. degree in computer science from Roskilde University, Roskilde, Denmark, in 2010. He was an Associate Professor with the Indian Institute of Technology Indore, India. Prior to the academic endeavor, he worked in the industry as a Chief Engineer (Research and Development) with the Advanced Technology Group, Samsung, India, and a Scientist Fellow in avionics at National Aerospace Laboratories, Bengaluru, India. He is currently an Associate Professor with the Center for Industrial Electronics, University of Southern Denmark, Denmark. Two (one in mobile phone systems and another in power electronics) of his inventions' disclosures have been granted patents. He works in (applied) robotics, autonomous vehicles, blockchain technology, cyber physical realtime embedded systems, digital transformation preserving trust and accountability, formal verification, industry X.0, the Internet of Things, power electronics, and realtime kernel design.

SATYENDRA R. NISHAD was born in Mumbai, India, in 1994. He received the Bachelor of Engineering (B.E.) degree in electronics and telecommunication engineering from the University of Mumbai, India, in 2015, and the Master of Technology (M.Tech.) degree in electronics and communication engineering (robotics) from the Defense Institute of Advanced Technology (DU), Pune, India, in 2019.

From 2019 to 2022, he was a Research Fellow with the Department of Mechanical Engineering, Indian Institute of Technology Patna, India. His research interests include mobile robotics, bio-inspired robotics, robot motion planning, and robot hardware design.

ATUL THAKUR (Member, IEEE) received the Bachelor of Engineering (B.E.) degree in production engineering from the University of Mumbai, in 2003, the Master of Technology (M.Tech.) degree in manufacturing engineering from the Indian Institute of Technology, Mumbai, in 2006, and the Ph.D. degree in mechanical engineering from the University of Maryland, College Park, MD, USA, in 2011. From 2011 to 2012, he was a Postdoctoral Research Associate with the Department of Mechanical Engineering, University of Maryland. He is currently an Associate Professor with the Department of Mechanical Engineering, Indian Institute of Technology Patna. His research interest includes physics-aware planning for robots interacting with unregulated and to some extent adverse physical environments.

• • •